Unveiling the Structural-Functional Interplay of Brain Networks in Depression: an Integrated DTI-fMRI Study

Federica Goffi[1], Elena Scalbi[1], Emma Tassi[2,1], Letizia Squarcina[3], Maria Pia Marra[2], Lorena Di Consoli[2], Adele Ferro[2], Giandomenico Schiena[2], Fabio M. Triulzi[4], Anna M. Bianchi[1], Paolo Brambilla[2,3], Eleonora Maggioni[1,2]

[1] Department of Electronics, Information and Bioengineering, Politecnico di Milano, Milan, Italy
[2] Department of Neurosciences and Mental Health,
Fondazione IRCCS Ca' Granda Ospedale Maggiore Policlinico, Milan, Italy
[3] Department of Pathophysiology and Transplantation, Università degli Studi di Milano, Milan, Italy
[4] Neuroradiology Unit, Fondazione IRCCS Ca' Granda Ospedale Maggiore Policlinico, Milan, Italy

***Abstract*—Diffusion tensor imaging (DTI) and functional magnetic resonance imaging (fMRI) are powerful neuroimaging techniques providing complementary information on brain structural (SC) and functional (FC) connectivity, respectively. Integrating them gives a deeper understanding of brain structural-functional interplay, which is particularly relevant in the search for brain markers of psychiatric illnesses like major depressive disorder (MDD). In this study, a novel DTI-driven fMRI approach was developed and preliminarily tested to identify any alterations in structural-functional network coupling in MDD. FC was estimated from DTI-derived features within a normative healthy control (HC) framework, using linear and quadratic models. SC strength, shortest path length, and physical distance showed significant influences on FC prediction in the linear model, whereas path length was non-significant in the quadratic version. The models were applied to a pilot test set of MDD and HC, comparing the predictive performance of the models between the two groups. The results showed reduced whole-brain similarity between estimated and measured FC in MDD vs. HC. These findings were confirmed on a smaller scale, showing significant differences in the model reconstruction error of ROI-to-ROI connectivity in key resting-state networks. These results suggest that altered brain structural-functional interactions may underlie MDD, providing new insights into potential biomarkers.**

***Index Terms*—DTI, fMRI, brain connectivity, multimodal integration, major depressive disorder.**

I. Introduction

In recent years, advances in neuroimaging techniques have revolutionized our understanding of intricate workings of the human brain, offering unparalleled insight into its structural and functional properties. Diffusion tensor imaging (DTI) and functional magnetic resonance imaging (fMRI) have emerged as powerful tools to study brain connectivity, each providing a complementary perspective. DTI focuses on examining the microstructural properties of white matter (WM), shedding light on structural connectivity (SC) [1]. Conversely, fMRI measures blood oxygen level-dependent (BOLD) signal fluctuations, associated with neural activity, providing a means to assess functional connectivity (FC) [2]. Given the inherently interconnection between white and grey matter, the integration of these modalities appears as a natural approach to investigate the interplay between brain structure and function, which is crucial for exploring cognitive and behavioral processes, and psychiatric diseases, such as major depressive disorder (MDD) [3]. Previous studies integrated these two modalities through different perspectives and based on different rationales, such as to facilitate SC studies, guide neurosurgical interventions, and construct functional correspondence using structural consistence. DTI/fMRI data fusion methods include fMRI-guided fiber tracking or filtering (fMRI assists DTI), functional analyses based on DTI-derived network (DTI assists fMRI), and joint DTI/fMRI analysis and modeling, in which both modalities play equally important roles [4]. Despite these advances, the brain structural-functional relationship remains partially unknown, especially in psychopathology. Within this context, MDD is a complex psychiatric disorder associated with disruptions in both SC and FC [3]. While studies have identified patterns of dysconnectivity, the underlying brain mechanisms remain elusive.

In this study, a new DTI-fMRI integration method is introduced. Using a DTI-driven fMRI approach, FC is inferred from a set of DTI-derived features in a normative framework of healthy young adults and subsequently applied to MDD patients. This cross-modality technique aims to identify possible deviations in SC-FC coupling in MDD, offering new insight into its neurobiological basis.

The study was supported by the European Union - NextGeneration EU (PRIN 2022 PNRR, grant n. P20229MFRC to FG), the Italian Ministry of University and Research ('Dipartimenti di Eccellenza' Programme 2023–27 - Dept. of Pathophysiology and Transplantation, Università degli Studi di Milano to PB), the Italian Ministry of Health (HLS-DA, PNC-E3-2022-23683266– CUP: C43C22001630001 / MI-0117 and Ricerca Corrente 2025 to PB), Fondazione Cariplo (grant n. 2019–3416 to PB), and ERANET Neuron JTC 2023 (ERP-2023-23684211 to PB).

Corresponding author: eleonora.maggioni@polimi.it

II. METHODS

A. Participants and study protocol

Twenty-two subjects (aged 36.6±11.8 years, 11 M and 11 F) were included in the study, 17 healthy controls (HC) and a pilot sample of 5 patients with MDD. Clinical diagnoses were assessed using the Italian version of the structured clinical interview for DMS-5. The exclusion criteria for all participants included intelligence quotient$<$70, lifetime abuse of alcohol or substances, history of head trauma with loss of consciousness, neurological and neurodegenerative disorders.

The participants underwent a MRI session using a 3T Philips Achieva DStream scanner (Philips, Best, The Netherlands) equipped with a 32-channel head coil. A structural brain image was acquired using a 3D T1-weighted TFE SENSE sequence (field of view (FOV): 250 mm (FH) x 240 mm (AP) x 180 mm (RL), voxel size: 1 x 1 x 1 mm^3, TE: 4 ms, TR: 8 ms, flip angle: 8°) and used as morphological reference. For diffusion weighted data, a SE-EPI sequence was applied (FOV: 120 mm (FH) x 256 mm (AP) x 256 mm (RL), voxel size: 2 x 2 x 2 mm^3, TR: 5.5 s, TE: 90 ms, flip angle: 90°). Diffusion was sampled along 64 directions with b-value=1000. Two additional reference volumes were acquired with no diffusion weighting (b-value=0). Two hundred fMRI volumes were collected during eyes-closed resting state using a multi-transmit T2*-weighted EPI sequence (FOV: 120 mm (FH) x 256 mm (AP) x 256 mm (RL), voxel size: 2 x 2 x 2 mm^3, echo time (TE): 30 ms, repetition time (TR): 2500 ms, flip angle: 90°). All subjects provided a written informed consent to the study protocol, which was approved by the Ethics Committee of Fondazione IRCCS Ca' Granda Ospedale Maggiore Policlinico, Milan, Italy, and was conducted in accordance with the Declaration of Helsinki.

B. Brain network definition

DTI and fMRI data were processed in parallel, and then the resulting unimodal SC and FC information was integrated in a cross-modality framework. Both connectivity matrices were derived using the same network nodes, which corresponded to standard regions of interest (ROI) of the automated anatomical labeling 3 (AAL3) atlas [5]. From the original set of 166 ROIs, cerebellum and vermis were excluded due to incomplete coverage in the FOV for some participants. Additionally, reuniens (thalamic nuclei) were omitted because their definition on a standard 0.5 mm^3 template was not adequately captured in the acquired imaging data. Consequently, a total of 138 ROIs were retained as nodes for the connectivity analyses.

C. DTI analysis

All preprocessing steps for DTI analysis were performed using FMRIB Software Library (FSL). Susceptibility-induced distortions in the DWI data were corrected with *topup*, while movement-related and eddy-current-induced artifacts were mitigated using *eddy*. The corrected DWI volumes were then used to reconstruct DTI data. Bedpostx was used to estimate the fiber distribution within each voxel via Bayesian estimation, modeling up to two main fiber orientations per voxel and accounting for the presence of crossing fibers. The estimated distributions informed a probabilistic tractography analysis to map structural connections between the 138 ROIs. Prior to tractography, the ROIs were transformed from standard space to diffusion space and used as seed masks for *probtrackx*. A distance correction was applied to compensate for connectivity attenuation with increasing tract length. The output from *probtrackx* consisted of a 3D probability map and the corresponding SC matrix. SC values underwent waytotal normalization to account for seed region size, and rescaled to a 0-1 range. The SC matrix generated by *probtrackx* was asymmetric, reflecting the directionality of structural connections between regions. A threshold was applied to retain only the top 20% of the strongest connections, after which the matrix was binarized and used to compute the shortest path length, defined as the number of links in the path connecting each ROI pair.

D. fMRI analysis

fMRI data preprocessing was carried out using the standard pipeline provided by HALFpipe toolbox [6]. The preprocessing steps encompassed realignment of fMRI volumes, co-registration with the anatomical image, segmentation of brain tissue, and spatial normalization to the MNI standard space. Additional commonly applied procedures were implemented, including spatial smoothing with a 6 mm FWHM kernel, grand mean scaling (mean=10,000), and Gaussian-weighted temporal filtering (width=0–125 s). A multi-metric comparison of additional denoising strategies was performed, leading to the regression of mean signals from white matter, cerebrospinal fluid, and the global signal [7]. fMRI volumes were then parceled using the AAL3 atlas, with BOLD signals extracted by averaging the signal across all voxels within each ROI. FC analysis was conducted using seed-based correlation to evaluate instantaneous temporal synchronization across brain regions. Pearson's correlation coefficients were computed for each pair of ROI-level BOLD signals.

E. DTI-fMRI integration

A DTI-informed approach was implemented using DTI information to drive the fMRI analysis. This method aimed to describe link-level FC as a function of SC-derived metrics while inherently considering the structural architecture. The DTI-driven fMRI method consisted of two main phases: model definition and cross-validation (CV) assessment, and final model training and testing.

Model design. A general linear model (GLM) was used as baseline framework to predict link-level FC through a set of anatomy-related features used as input. The model was termed "link-level" because each data point in the input set corresponded to a ROI-to-ROI connection. Two different model designs were considered: a `linear` model, using only first-order terms of the regressors, and a `purequadratic` version, using both first- and second-order terms. The independent variables within the GLM design matrix, each of them associated with a β coefficient, included SC between two ROIs

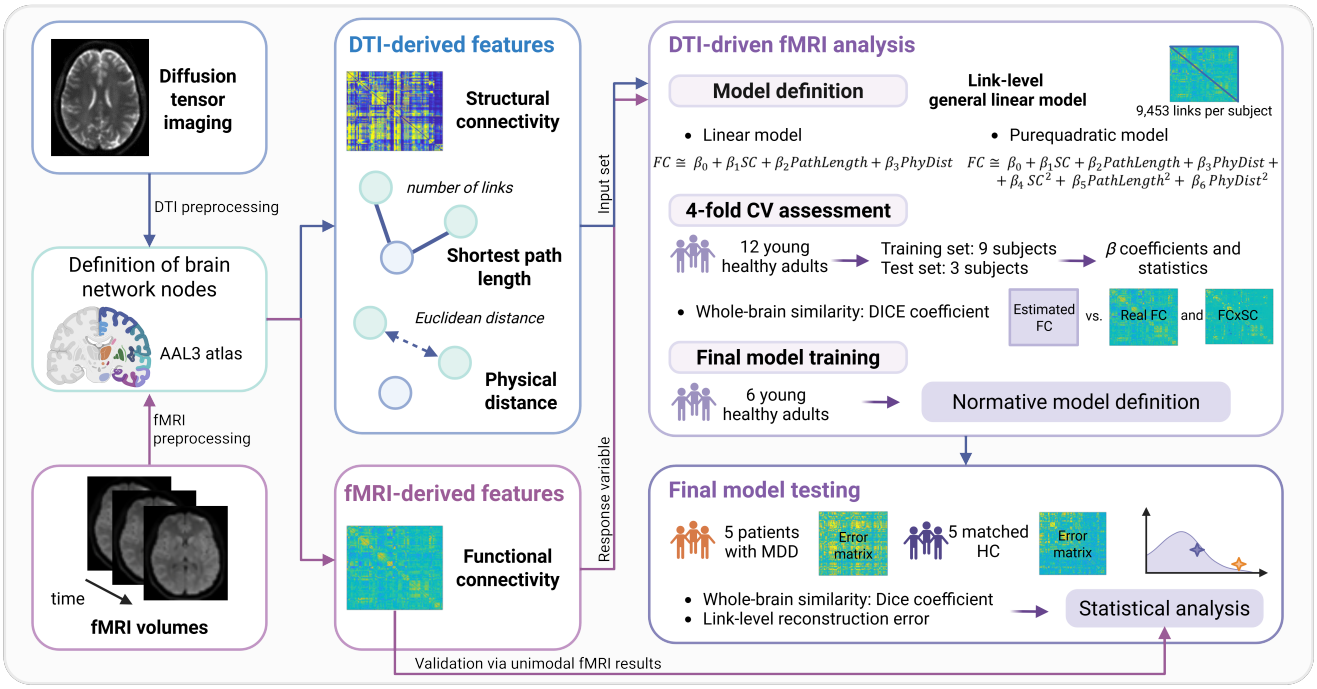

Fig. 1. DTI-fMRI integration.

(quantifying the WM tract strength), the reciprocal of shortest path length, and the reciprocal of the physical Euclidean distance between the barycenters of two ROIs. The dependent variable was the absolute FC value. Given the symmetry of the FC matrix, only the upper triangular section was considered for modeling. Instead, for SC values, the largest value between SC$a \rightarrow b$ and SC$b \rightarrow a$ was used, making the SC measure independent of directionality. The equations of the `linear` and `purequadratic` models are reported in Fig. 1.

The model was trained on a homogeneous dataset comprising 12 HC (6 M and 6 F) aged between 26 and 29 years. This process established a normative model, which serves as reference framework for modeling reference patterns within a control population, aiding in the detection and interpretation of deviations in other groups [8]. By mapping SC features to FC patterns in the HC cohort, the model aimed to infer the relationship between FC and SC in young healthy adults.

CV assessment. Model performance was evaluated using k-fold CV with k=4. Each fold consisted of a training set of 9 subjects and a validation set of 3 subjects, with each subject contributing with 9,453 observations. To mitigate biases arising from the small sample size and subject-specificity, three separate models were trained per fold, each comprising 28,359 random observations uniformly distributed across the 9 training subjects. The validation was based on the average of the estimated coefficients. The performance of the two models was assessed in the test CV folds using two primary measures: i) statistical significance of the β coefficient estimates, assessed via p-values, and ii) similarity between estimated FC and observed FC, measured using the Dice coefficient on binarized connectivity matrices (retaining the 40% strongest connections). For the second metric, the modeled FC was compared against both the empirical FC and the empirical FCxSC matrix, which was derived by element-wise multiplication of FC and SC values, thus emphasizing FC connections supported by strong WM pathways and highlighted SC pathways that aligned with resting-state functional activity.

Model training. Following CV assessment, the final `linear` and `purequadratic` models were trained on data points from half of the initial training dataset (6 homogeneous HC), and tested on the remaining half for consistency.

Model test on diagnosis. The trained `linear` and `purequadratic` models were subsequently tested on a pilot sample of 5 MDD patients (aged 46.6 ± 7.9 years, 2 M and 3 F) (`test_MDD`) and on a matched sample of 5 HC (aged 49.2 ± 8.6 years, 3 M and 2 F) (`test_HC`) to evaluate potential diagnosis deviations in the structural-functional coupling compared to the normative pattern, removing age- and sex-related variability. The models' performance was quantified on the basis of the whole-brain similarity between the estimated and observed FC, using the Dice coefficient on binarized matrices. Additionally, reconstruction error at the link level was computed as the pointwise difference between estimated and measured FC values. These metrics were calculated separately for `test_MDD` and `test_HC` sets. Group-level analyses were performed using a statistical GLM approach, with age, sex, and diagnosis as covariates, and Dice coefficients or reconstruction errors as dependent variables.

Finally, a group-level fMRI analysis was conducted using a GLM with age, sex, and diagnosis as covariates, and mea-

sured FC values as response variable. This analysis aimed to compare the results obtained using the normative DTI-driven FC model against those derived from unimodal FC.

III. Results and discussion

The implemented DTI-driven fMRI framework defined a cross-modality method to estimate FC from a set of SC features, and to identify any MDD deviations from the normative model.

Model performance. The p-values associated with the β coefficients for `linear` and `purequadratic` models are reported in Table I and II, respectively. For the `linear` model, all structural parameters (SC, path length and physical distance) showed a significant effect on FC prediction (p-value$<$0.05). Conversely, when second-order terms were included, the relevance of ROI-to-ROI distance decreased, as shown by the non-significant p-values for path length regressors.

TABLE I
LINEAR MODEL: ESTIMATED GLM COEFFICIENTS AND STATISTICS

Regressor	**4-fold CV**		**Final model**	
	β	*p-value*	β	*p-value*
Intercept	0.11	≈ 0	0.11	≈ 0
SC	0.08	8.98e-05	0.06	3.00e-03
PathLength	0.03	6.74e-07	0.02	1.48e-04
PhyDist	0.36	4.69e-124	0.37	2.20e-138

TABLE II
QUADRATIC MODEL: ESTIMATED GLM COEFFICIENTS AND STATISTICS

Regressor	**4-fold CV**		**Final model**	
	β	*p-value*	β	*p-value*
Intercept	0.13	5.76e-251	0.12	5.31e-248
SC	0.42	2.64e-17	0.45	3.33e-20
PathLength	-0.03	0.13	-0.03	0.12
PhyDist	0.12	2.96e-14	0.12	1.51e-05
SC^2	-0.65	7.06e-04	-0.73	7.07e-17
$PathLength^2$	0.02	0.16	0.02	0.21
$PhyDist^2$	0.47	2.74e-19	0.48	1.27e-21

Table III presents similarity results for both models, quantifying their ability to reconstruct FC matrix by comparing it to the measured FC and the combined FCxSC matrix. The results showed that both models perform similarly in reconstructing FC matrix, suggesting that incorporating quadratic terms for SC and physical distance can efficiently replace the information carried out by path length regressors, which were not significant in the `purequadratic` model.

TABLE III
SIMILARITY RESULTS

Modeled FC vs.	**Measured FC**	**FCxSC**
Linear model	41.8%	66.2%
Purequadratic model	41.7%	71.3%

Notably, both models integrated structural information when modeling FC, as shown by the higher similarity between the reconstructed connectivity matrix and FCxSC, compared to its similarity with measured FC. These findings indicate that both approaches capture functional and structural network characteristics, offering a more comprehensive representation of brain connectivity.

Model test on diagnosis. The models were trained in a normative fashion and their performance was assessed to test for diagnosis effect. The coefficients of the final models, consistent with those obtained during 4-fold CV, and the corresponding p-values are presented in Table I and II.

In the test sets, the prediction performance at the whole-brain level, assessed by the Dice coefficient, revealed that the similarity between real and modeled FC was significantly lower in MDD patients compared to HC for the `purequadratic` model and trended toward significance for the `linear` model, as shown in Table IV. This finding suggests that MDD has a significant impact on the structure-function brain connectivity relationship. In contrast, no significant effects were observed for age or sex regressors (p-value$>$0.05).

TABLE IV
MODEL TEST: DICE COEFFICIENT RESULTS

Covariate	**Linear**		**Purequadratic**	
	t-stat	*p-value*	*t-stat*	*p-value*
Intercept	11.12	3.15e-05	14.30	7.31e-06
Age	0.40	0.52	0.37	0.73
Sex	0.93	0.39	0.94	0.38
Diagnosis	-2.38	0.054	-2.63	0.039

When evaluating the model performance at the link level, MDD showed a significant effect on pointwise reconstruction error (p-value$<$0.001) for both `linear` and `purequadratic` models. Significant differences in the brain structural-functional interplay between MDD and HC were observed in links belonging to important resting-state networks as the default mode and salience networks, in interaction with areas of the limbic systems, all structures that are involved in MDD psychopathology (see Table V and VI).

The link-level results derived from the `linear` and the `purequadratic` models are consistent in terms of diagnosis-related differences, supporting the framework robustness. The significant links that are distinct between the two versions suggest deviations in SC and physical distance between the two ROIs rather than in the path length, which was not significant in the `purequadratic` model. The comparison of overlap between DTI-derived and unimodal fMRI findings (in Table VII) offers deeper insights into brain function-anatomy interdependencies. While overlapping results in fMRI and DTI-fMRI analyses likely reflect functional alterations, differences identified in the DTI-driven fMRI analysis but absent in the fMRI analysis may be linked to structural alterations. This interpretation is supported by the observation that inaccurate FC predictions arise when derived from altered SC-related information, as evidenced by the higher variance in FC prediction observed for the same link in MDD vs. HC.

TABLE V
LINEAR MODEL: SIGNIFICANT RECONSTRUCTION ERRORS FOR DIAGNOSIS

Label ROI 1	Label ROI 2	*t-stat*	*p-value*
Precentral L	Temporal Sup R	-7.21	3.58e-04
Frontal Mid 2 L	Thal Pul R	6.27	7.68e-04
Frontal Inf Tri R	Putamen L	-5.99	9.73e-04
Frontal Inf Orb 2 L	Hippocampus L	6.38	6.96e-04
Supp Motor Area L	Occipital Mid L	-6.26	7.69e-04
OFClat L	Precunes R	7.08	3.96e-04
OFClat L	Temporal Pole Sup R	7.85	2.26e-04
Insula R	Thal MGN L	-7.29	3.37e-04
ParaHippocampal L	VTA L	7.11	3.88e-04
Parietal Sup R	Temporal Pole Mid L	6.97	4.33e-04
Paracentral Lobule R	Thal MGN L	-7.12	3.85e-04
Paracentral Lobule R	Thal$_I L_R$	-6.61	5.76e-04
Putamen L	Thal LP R	-6.33	7.27e-04
Putamen R	Red N L	6.21	8.05e-04
Temporal Sup R	LC R	-6.20	8.09e-05
Thal LP L	ACC sub L	6.40	6.88e-04
ACC sup L	Red N L	-6.51	6.26e-04

TABLE VI
QUADRATIC MODEL: SIGNIFICANT RECONSTRUCTION ERRORS FOR DIAGNOSIS

Label ROI 1	Label ROI 2	*t-stat*	*p-value*
Precentral L	Temporal Sup R	-7.28	3.43e-04
Frontal Sup 2 R	Thal Pul R	6.63	5.67e-04
Frontal Inf Orb 2 L	Hippocampus L	6.09	8.88e-04
Supp Motor Area L	Occipital Mid L	-6.17	8.30e-04
OFClat L	Precunes R	7.04	4.09e-04
OFClat L	Temporal Pole Sup R	7.83	2.28e-04
Insula R	Thal MGN L	-6.92	4.50e-04
ParaHippocampal L	Temporal Pole Mid L	-6.14	8.50e-04
ParaHippocampal L	VTA L	6.59	5.85e-04
Parietal Sup R	Temporal Pole Mid L	6.86	4.69e-04
Paracentral Lobule R	Thal MGN L	-6.71	5.28e-04
Putamen L	Thal LP R	-6.21	8.07e-04
Putamen R	Red N L	6.08	8.97e-04
Temporal Sup R	LC R	-6.18	8.22e-05
Thal LP L	ACC sub L	6.29	7.50e-04
Thal LP R	Thal VL L	-6.02	9.44e-04
ACC sup L	Red N L	-6.55	6.08e-04

TABLE VII
UNIMODAL FMRI RESULTS FOR DIAGNOSIS

Label ROI 1	Label ROI 2	*t-stat*	*p-value*
Precentral L	Temporal Sup R	-6.03	9.42e-04
Frontal Mid 2 L	Thal Pul R	6.58	5.93e-04
Frontal Inf Orb 2 L	Hippocampus L	6.50	6.33e-04
Rolandic Oper R	Thal VPL L	-6.41	6.78e-04
Olfactory R	Thal MGN L	-6.25	7.75e-04
OFClat L	Temporal Pole Sup R	7.04	3.13e-04
Insula R	Thal MGN L	-7.07	3.99e-04
ParaHippocampal L	Temporal Pole Mid L	-6.15	8.46e-04
ParaHippocampal L	Thal AV L	-7.95	2.11e-04
ParaHippocampal L	Thal PuA L	-7.51	2.88e-04
Fusiform R	Red N L	7.22	3.55e-04
Pallidum L	ACC pre L	-6.10	8.84e-04
Temporal Inf R	ACC sub L	6.78	5.01e-04
Temporal Inf R	LC R	-7.87	2.21e-04
Thal LP L	Acc sub L	6.77	5.07e-05
Thal LP R	Thal VL L	-6.88	4.64e-04
Thal VL R	Thal MDm L	-6.61	5.75e-04
ACC sup L	Red N L	-6.18	8.24e-04

IV. CONCLUSIONS

In this study, we introduced an innovative integrated DTI-fMRI approach to explore the complex structural-functional interplay in brain networks. This method enabled the definition of a novel representation of FC that intrinsically incorporates structural information, as evidenced by the significant effects of the predicting variables. A key strength of our approach lies in its interpretability, a crucial factor in clinical biomarker identification. However, future advances including larger datasets and more sophisticated models, as deep learning algorithms, will facilitate the exploration of more intricate dependencies. Training our DTI-driven fMRI model in a healthy cohort allowed us to establish a normative framework against which subject-specific alterations in clinical populations can be assessed. Our preliminary findings suggest that similarity between predicted and measured FC is significantly reduced in MDD, potentially indicating disrupted anatomical-functional coupling in brain networks. Notably, regions implicated in MDD exhibited higher reconstruction errors, reinforcing the validity of our results [3]. Altered structural-functional coupling was observed within circuits involved in depressive mechanisms, including the default mode and salience networks, as well as reward, cognitive control and limbic circuits. These findings align with previous research demonstrating hyperconnectivity in the default mode network in MDD, which was linked to excessive rumination, negative thoughts, and heightened self-referential processing [9]. In conclusion, our preliminary results support the validity of integrating DTI and fMRI information, including the conversion of DTI-related features into a new FC measure, to uncover the structural-functional link in brain networks. This framework holds promise for both physiological and psychopathological investigations, paving the way for identifying neuroimaging-based markers for MDD.

REFERENCES

[1] B. Q. Rosen and E. Halgren, "A whole-cortex probabilistic diffusion tractography connectome," *eNeuro*, vol. 8, no. 1, 2021.

[2] M. H. Lee, C. D. Smyser, and J. S. Shimony, "Resting-state fMRI: a review of methods and clinical applications," *AJNR American Journal of Neuroradiology*, vol. 34, pp. 1866–1872, October 2013.

[3] Z. Li, M. Ruan, J. Chen, and Y. Fang, "Major depressive disorder: Advances in neuroscience research and translational applications," *Neuroscience Bulletin*, vol. 37, pp. 863–880, 2021.

[4] D. Zhu *et al.*, "Fusing DTI and fMRI data: a survey of methods and applications," *NeuroImage*, vol. 102 Pt 1, pp. 184–191, Nov 2014.

[5] E. T. Rolls, C.-C. Huang, C.-P. Lin, J. Feng, and M. Joliot, "Automated anatomical labelling atlas 3," *NeuroImage*, vol. 206, p. 116189, 2020.

[6] L. Waller *et al.*, "ENIGMA HALFpipe: Interactive, reproducible, and efficient analysis for resting-state and task-based fMRI data," *Human Brain Mapping*, vol. 43, no. 9, pp. 2727–2742, 2022.

[7] F. Goffi, A. M. Bianchi, G. Schiena, P. Brambilla, and E. Maggioni, "Multi-metric approach for the comparison of denoising techniques for resting-state fMRI," *Human Brain Mapping*, 2025.

[8] A. Marquand, I. Rezek, J. Buitelaar, and C. Beckmann, "Understanding heterogeneity in clinical cohorts using normative models: Beyond case-control studies," *Biological Psychiatry*, vol. 80, pp. 552–561, 2016.

[9] L. M. Williams, "Defining biotypes for depression and anxiety based on large-scale circuit dysfunction: a theoretical review of the evidence and future directions for clinical translation," *Depression and Anxiety*, vol. 34, no. 1, pp. 9–24, 2017.